Nano Energy 115 (2023) 108674

Contents lists available at ScienceDirect

Nano Energy

journal homepage: www.elsevier.com/locate/nanoen

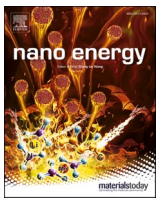

High-loading of organosilane-grafted carbon dots in high-performance luminescent solar concentrators with ultrahigh transparency

Jiurong Li [a], Jiancang Chen [a], Xiujian Zhao [a], Alberto Vomiero [b,c,*], Xiao Gong [a,**]

[a] State Key Laboratory of Silicate Materials for Architectures, Wuhan University of Technology, Wuhan 430070, PR China
[b] Division of Materials Science, Department of Engineering Sciences and Mathematics, Luleå University of Technology, 971 87 Luleå, Sweden
[c] Department of Molecular Sciences and Nanosystems, Ca' Foscari University of Venice, Via Torino 155, 30172 Venezia Mestre, Italy

ARTICLE INFO

Keywords:
Luminescent solar concentrators
Organosilane-grafted carbon dots
UV shielding
Highly transparent
High-loading

ABSTRACT

Carbon dots (CDs) generally suffer from aggregation-induced fluorescence quenching effect in solid-state, which significantly limits their application in photoelectric devices. Due to this effect, it is a great challenge to achieve high-transparency and high-performance luminescent solar concentrators (LSCs) based on CDs. Here, the synthesis of organosilane-grafted carbon dots (Si-CDs) is rationally designed by hydrothermal method using anhydrous citric acid, ethanolamine and KH-792 as the reaction precursors. The obtained Si-CDs can be uniformly dispersed in the polyvinyl alcohol (PVA) matrix through the dehydration condensation reaction and hydrogen bonding between the silicon hydroxyl group of Si-CDs and the hydroxyl group of PVA. Based on this property, Si-CDs/PVA thin-film LSCs ($5 \times 5 \times 0.2$ cm^3) with ultrahigh CD loading (25 wt%) and high transparency can be fabricated, exhibiting excellent absorption in the UV spectral region and about 90 % transmission in the visible range. Furthermore, the power conversion efficiency (PCE) of the LSCs can reach 2.09 % under a standard solar light and shows excellent stability even over 12 weeks. This synthetic design is expected to be beneficial for future development of CD synthesis and paves the way for the development of CDs-based photoelectric devices.

1. Introduction

Luminescent solar concentrators (LSCs), as a new type of solar collector, have superior flexibility in form design, such as changeable shape, color, size, and transparency, etc [1,2]. Also, LSCs possess low cost, as they can reduce the cost of solar power generation via reducing the utilization of expensive photovoltaic materials (e.g., monocrystalline silicon). These excellent properties allow LSCs to be applied to buildings in the future to realize photovoltaic building integration (solar windows, solar curtain walls, solar roofs, etc.) [1,3]. LSCs are mainly fabricated by embedding a fluorescent material in a waveguide matrix or by mixing it with a film-forming agent and coating it on the waveguide surface. These waveguides containing embedded fluorescent materials absorb sunlight and then the fluorophores re-emit photons, which are guided by total internal reflection to the photovoltaic devices located at their edges for conversion into effective electrical energy [4–6]. Thus, the selection of fluorescent materials is extremely critical to achieve high-performance LSCs devices. Currently, the fluorescent materials employed in LSCs include organic dyes, semiconductor nanocrystals, perovskite quantum dots, and carbon dots (CDs) [7,8]. Recently, CDs have been widely adopted as fluorescent materials for LSCs due to their excellent properties such as tunable absorption/emission spectra, high quantum efficiency, easy synthesis, adjustable Stokes shift and low toxicity [4,5,9–19].

Actually, CDs usually undergo aggregation-induced fluorescence quenching (ACQ) effect in the solid state, which limits their application in many solid-state light-emitting devices. An advantageous way to effectively avoid the ACQ effect is to disperse CDs in polymeric matrices. For example, CDs can simply be physically dispersed in polymers such as polyvinylpyrrolidone (PVP), polyvinyl alcohol (PVA), and polymethyl methacrylate (PMMA). Unfortunately, high loading of CDs in polymer matrix can also cause ACQ effect or even phase separation. To effectively avoid ACQ effect and phase separation due to high concentration of CDs, the loading of CDs in polymers is generally not higher than 10 wt% [20]. More critically, a higher loading of CDs in the polymer can be more beneficial to collect more solar energy in the practical application of

* Corresponding author at: Division of Materials Science, Department of Engineering Sciences and Mathematics, Luleå University of Technology, 971 87 Luleå, Sweden.
** Corresponding author.
E-mail addresses: alberto.vomiero@ltu.se (A. Vomiero), xgong@whut.edu.cn (X. Gong).

https://doi.org/10.1016/j.nanoen.2023.108674
Received 24 May 2023; Received in revised form 3 July 2023; Accepted 4 July 2023
Available online 10 July 2023

LSCs. Thus, low loading of CDs in polymers will seriously affect the photovoltaic performance of LSCs. Although the research on fluorescent materials and optical waveguide materials related to LSCs has been well achieved, how to obtain higher loading of fluorescent materials in optical waveguide matrix has become a pressing challenge, which plays a crucial role in further improving the performance of LSCs. Yuan et al. [20,21] proposed in situ cross-linked organosilanes to modify CDs with organosilanes as the film-forming agent (KH-792) to prepare green LSCs with high CDs loading, but the size dimension was only 30 mm × 30 mm × 3 mm. Later, Wang et al. [22] even dispersed the synthesized silicon CDs in two dendritic silicone polymers with good compatibility, resulting in a 10 % higher loading of CDs in LSCs than previously reported and an external optical efficiency of 7.58 % for LSC devices with the same size dimension of 25 × 25 × 1 mm. These reports all suffered from the small size of the device and its extremely low transparency that seriously hinder the development of LSCs. Therefore, rational design adopting CDs chemically dispersed in polymer matrix to improve the loading of CDs in LSCs has not been fully achieved yet, which is conducive to boosting the development of LSCs for a widespread application.

In this work, organosilane-grafted CDs (Si-CDs) were synthesized directly by hydrothermal method in one step using anhydrous citric acid, ethanolamine and KH-792 as raw materials. The obtained Si-CDs had a size of about 4.35 nm and a photoluminescence quantum yield (PLQY) of 57.77 %. Si-CDs/PVA thin-film LSCs (5 × 5 × 0.2 cm^3) with high CDs loading (25 wt%) were prepared through the chemical dispersion of the Si-CDs in PVA matrix via the dehydration condensation reaction between the silicon hydroxyl group of the Si-CDs and the hydroxyl group of PVA and hydrogen bonding through the adoption of water-soluble PVA as the film-forming agent. The Si-CDs possessed excellent UV shielding properties after interacting with PVA. In fact, the prepared CDs have strong absorption in the UV region and thus achieve the function of UV shielding, by protecting the area underneath. At the same time, the strong light absorption is also beneficial to enhance the performance of LSCs devices, by increasing the number of re-emitted photons, which can be collected at the border of the LSC slab. The prepared Si-CDs/PVA thin-film LSCs exhibited excellent absorption performance not only in the UV portion but also in the visible portion with a transmittance of up to 90 % in the 400–800 nm spectral region. Furthermore, the PCE of the Si-CDs/PVA thin-film LSC could reach 2.09 % under a standard solar light (AM 1.5 G, 100 mW cm^{-2}) and exhibited good device performance stability. This synthetic strategy is prospective to provide favorable technical support in future CDs-based LSC devices.

2. Experiments and methods

2.1. Materials

Citric acid anhydrous (CA), N-[3-(trimethoxysilyl)propyl]ethylenediamine (KH-792), concentrated hydrochloric acid (HCl) purchased from Aladdin Chemistry Co., Ltd., China. Ethanolamine (EA), petroleum ether (PE) and anhydrous ethanol (EtOH) were procured from Sinopharm Chemistry Reagent Co., Ltd., China.

2.2. Synthesis of Si-CDs

Briefly, 0.42 g of CA and 3 mL of deionized water were added to a 20 mL beaker and ultrasonically dispersed for 10 min to obtain a colorless and transparent solution after complete dissolution of CA. Then, 3 mL of KH-792 were added to the above solution and stirred magnetically for 10 min, followed by the addition of 300 μL of EA and continuous stirring for 10 min. After that, the mixed solution in the beaker was transferred to 25 mL Teflon liner, then sealed with stainless steel reactor liner and placed in an electric blast oven at 200 °C for 5 h. After the reaction was finished, the reactor was taken out and cooled to room temperature naturally to obtain a yellow reaction solution. Immediately after the reaction, 34 mL of PE were added to the reaction solution, and the solution was centrifuged repeatedly at 8000 rpm for several times to remove the residual KH-792. The centrifuged solution was briefly filtered using a 0.22 μm filter membrane to remove large particles, and finally the filtered solution was further dialyzed for 12 h using a dialysis bag with a molecular weight of 1000 Da to remove the free small molecules and unreacted reactants during the synthesis process, and concentrated by rotary evaporation.

2.3. Preparation of Si-CDs/PVA thin film based LSCs

Firstly, an aqueous solution of PVA was prepared. Briefly, 9 g of PVA and 60 mL of deionized water were heated and stirred rapidly at 90 °C for 12 h, and then stirred slowly at low speed for 12 h. The resulting PVA solution was then sonicated for 30 min to remove air bubbles from the PVA solution. The PVA solution was then divided into five equal portions of 6 mL to be set aside. Secondly, a mixture of Si-CDs/PVA was prepared. Briefly, five different masses of Si-CDs (5 wt%, 10 wt%, 25 wt %, 45 wt% and 70 wt%) were weighed and added to each of the above five PVA solutions. Besides, 100 μL of HCl (1 M) was added to each of the mixed solutions because the acidic environment helps the hydrolysis of the silane and the mutual attraction of the hydroxyl groups of the PVA and the silicon hydroxyl groups of the Si-CDs. Lastly, the mixed solutions were magnetically stirred at room temperature for 24 h to obtain well-mixed Si-CDs/PVA coating solutions of different concentrations. Finally, Si-CDs/PVA thin film based LSC devices were prepared. Briefly, five different concentrations of Si-CDs/PVA mixed solutions were applied to the pre-prepared glass plate by an appropriate amount of drops respectively, minimizing the introduction of air bubbles during the drop coating process. After drop coating, the LSCs should be stored in a closed space at room temperature for a period of time (about one week). After the storage at room temperature, the incompletely dried films were then dried in a blast oven at 50 °C for 6 h to obtain the completely dried Si-CDs/PVA film type LSCs.

2.4. Characterizations

The morphology and structure of the Si-CDs were characterized by a field emission high-resolution transmission electron microscope (TEM) (model JEM-2100F) from Japan Electronics Corporation. The surface morphology and cross-sectional morphology of the Si-CDs/PVA thin-film LSCs were characterized by a cold field emission scanning electron microscope (SEM) with X-Max N80 energy spectrometer, model JSM-7500F, from Japan Electronics Corporation. The instrument employed for the surface morphology and roughness of the Si-CDs/PVA thin-film LSCs was a Nanoscope IV scanning probe microscope (atomic force) (AFM) from VEECO, USA, with a lateral resolution of < 0.2 nm. The instrument utilized for the crystal phase analysis of the samples was a D8 Advance X-ray diffractometer (XRD) from Bruker AXS, Germany, with X-rays Cu-Kα (λ = 0.15418 nm) radiation source, with a diffraction angle range of 10–90°. The instrument chosen for the infrared spectroscopy of the samples was a Fourier transform infrared (FTIR) spectrometer model Nicolet 6700 from THERMO ELECTRONS CIENTIFICINS TRUMENTS, USA. The X-ray photoelectron spectra (XPS) of Si-CDs were measured by an ESCALAB 250Xi X-ray photoelectron spectrometer manufactured by Thermo Fisher Scientific, Inc. UV–visible absorption and transmission spectra of the Si-CDs solution and Si-CDs/PVA thin film LSCs were measured with a UV–visible-NIR spectrophotometer model UV-2600 from Shimadzu, Japan, in the range of 250–800 nm. The fluorescence spectra of Si-CDs solution and Si-CDs/PVA film based LSC were performed with a time-resolved fluorescence spectrometer, model QM/TM/NIR, from Photon Technology International, USA. The fluorescence lifetime of the Si-CDs solution and Si-CDs/PVA film based LSC were measured by a time-resolved fluorescence spectrometer FL-TCSPC from HORIBA Jobin Yvon, France, which uses the time-correlated single photon counting (TCSPC) principle to record the decay of fluorescence

intensity of the sample with time. Photovoltaic properties of the LSCs were obtained with a solar simulator (IV4112, Newport Corp., Irvine, CA, USA) at an intensity of 100 mW cm^{-2} (1 sun), calibrated through a calibrated silicon solar cell. For the purpose, Si solar cells were integrated on the lateral side of the LSC. The integration of solar cells on the lateral side of LSCs was carried out in a way, which excludes the possibility for the light from the solar simulator to enter directly into the cell due to partial exposure of cell area to the air. This is a critical aspect, when evaluating the performance of LSC, not to overestimate photoconversion efficiency due to spurious light entering the solar cell directly during the measurement. Specifically, after the custom-sized Si photovoltaic cell was attached on one edge of the LSC by glass glue, the rest of the edges were uncovered. The uncovered part of the photovoltaic cell was blocked by the black tapes to avoid any incident light. Then the LSC was placed under a conventional AM 1.5 G solar simulator with illumination perpendicular to the surface of the LSC. No reflector or back diffuser was put beneath the device. The current-voltage curves were recorded through a multimeter (IV4112, Newport Corp., Irvine, CA, USA). The Si solar cells were measured also under direct simulated solar light at normal incidence to characterize their response to solar light.

3. Results and discussions

The microscopic morphology and size distribution of the Si-CDs were characterized and analyzed by TEM. Fig. 1**a** shows the TEM images of the Si-CDs, and it can be observed that the Si-CDs have a spherical-like structure and narrow particle dispersion. Additionally, the high-resolution TEM (HR-TEM) images of the Si-CDs (inset in the upper right corner of Fig. 1**a**) show that Si-CDs have high crystallinity with lattice stripe spacing of about 0.21 nm, which corresponds to the (100) inter-planar lattice spacing of graphite, indicating that the Si-CDs had a certain graphite-like crystal structure [23–27]. Fig. 1**b** shows the particle size distribution of the Si-CDs obtained from the TEM image by particle size statistics, from which it can be seen that the particle size of the Si-CDs ranged from 2 nm to 7 nm, and its average particle size was approximately 4.35 nm. To further investigate the structure of the Si-CDs, the XRD characterization was performed. A broad diffraction peak near 21.8° can be clearly seen in Fig. 1**c**, which is attributed to the amorphous carbon derived from the deformation caused by heteroatom dopants or sp^3 carbon defects in the graphite structure, indicating that the Si-CDs has a certain crystalline structure in addition to amorphous domains. The chemical structure of the Si-CDs was further investigated by FT-IR spectroscopy. As shown in Fig. 1**d**, the peaks appearing at approximately 3418 cm^{-1} and 3293 cm^{-1} are assigned to O–H and N–H stretching vibrations, respectively, which indicated that the Si-CDs exhibited a large number of hydroxyl and amino functional groups [28]. The peaks at 2933 cm^{-1} and 2883 cm^{-1} can be attributed to C–H stretching vibrations [29]. The peak at 1560 cm^{-1} can be ascribed to C═O vibrations. The existence of the characteristic peak of CO–NH bond at 1653 cm^{-1} proved that the amide bond was formed by the reaction of carboxyl and amino groups during hydrothermal process [28]. The chemical structure of the synthesized Si-CDs materials does not have C═C bonds, but the appearance of the characteristic peak at 1471 cm^{-1} caused by C═C stretching vibrations indicated that the raw material underwent a carbonization process at high temperature and pressure, as confirmed by TEM analysis [30]. The occurrence of Si–O–Si and Si–O–C stretching vibration peaks at 1125 cm^{-1} and 1035 cm^{-1} and the characteristic peak caused by Si–OH vibration at 929 cm^{-1} proved that the Si-CDs achieved surface organosilane functionalization [28]. The results of FT-IR spectroscopy revealed the abundance of hydroxyl, silicon hydroxyl, amino, and amide groups on the Si-CDs surface, which demonstrated the hydrophilic nature of the prepared Si-CDs that facilitated their dispersion in PVA polymers with hydrophilic properties.

The results of FT-IR spectroscopy of the Si-CDs can be further confirmed by XPS analysis. As shown in Fig. 2**a**, the XPS survey spectrum of the Si-CDs indicates that the main components of Si-CDs are four

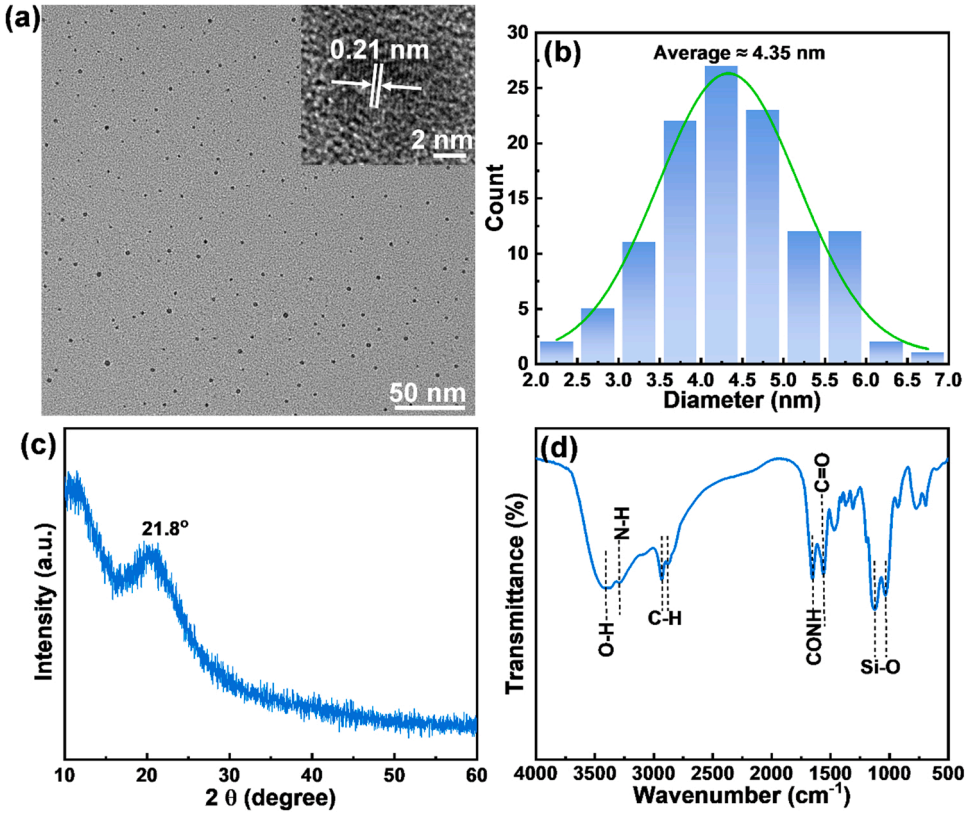

Fig. 1. (a) TEM image of the Si-CDs (inset: HR-TEM image of individual Si-CD). (b) The size distribution of the Si-CDs. (c) XRD pattern of the Si-CDs. (d) FT-IR spectrum of the Si-CDs.

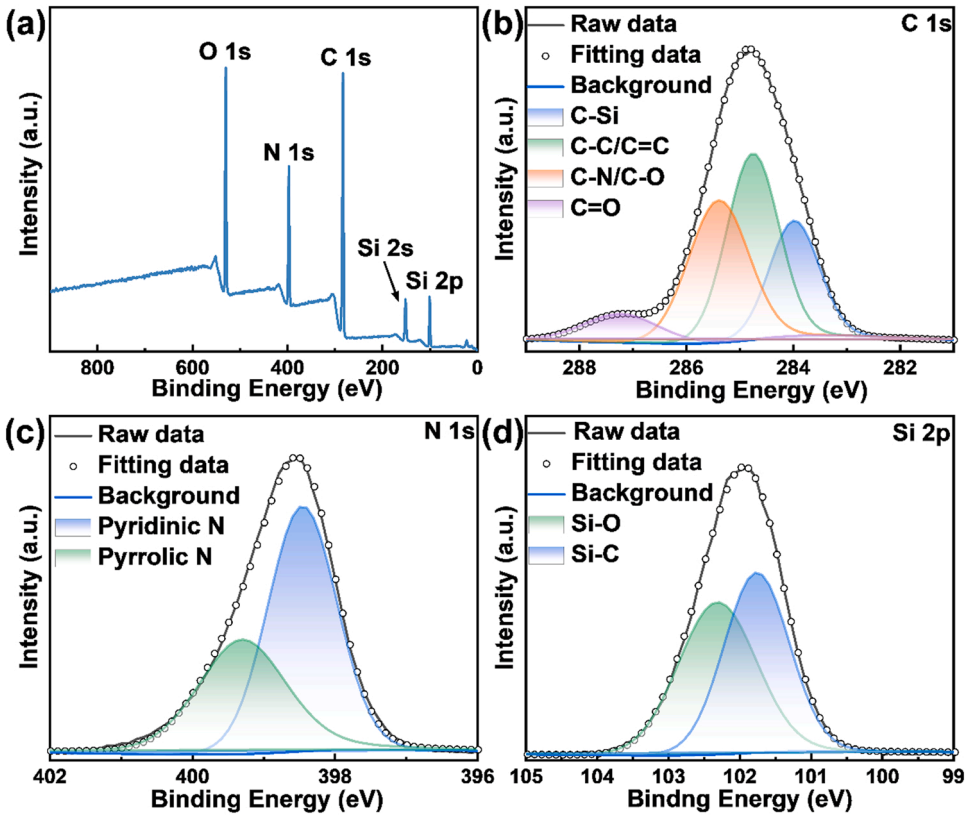

Fig. 2. XPS full scan of the Si-CDs (a). HR-XPS spectrum of (b) C 1s, (c) N 1s, (d) Si 2p.

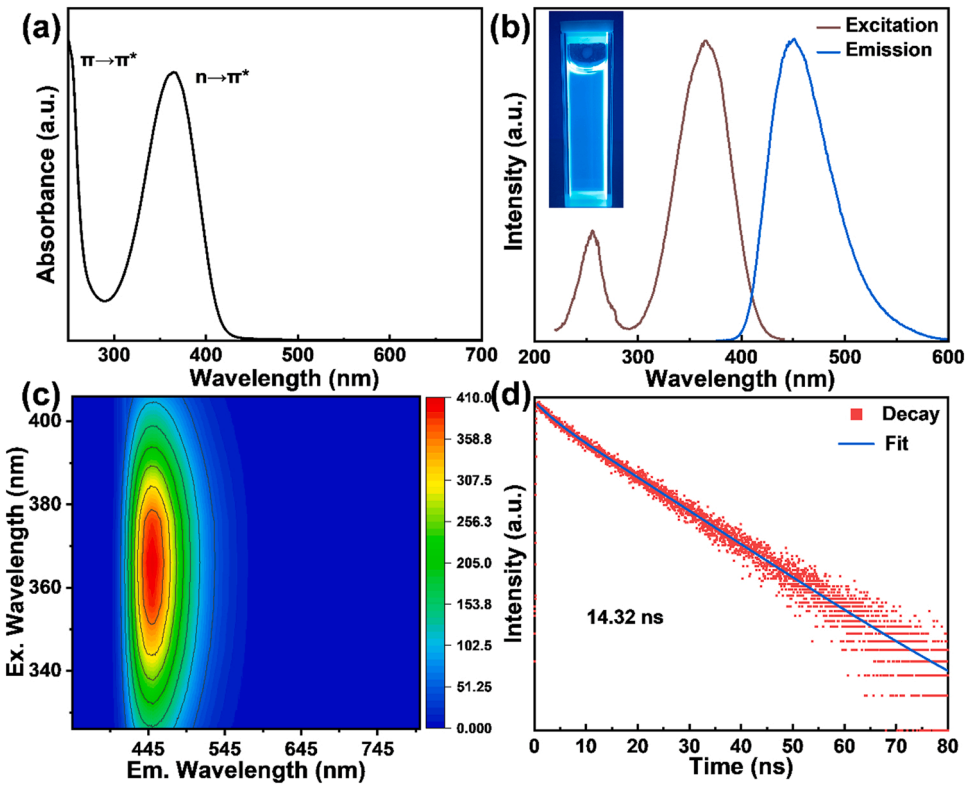

Fig. 3. (a) UV–vis absorption spectrum and (b) PL spectrum (excitation spectrum, λ_{em} = 450 nm, and emission spectrum, λ_{ex} = 366 nm) of a Si-CDs aqueous solution (inset is the photograph of Si-CDs aqueous solution under UV light irradiation). (c) Two-dimensional (2D) excitation-emission mapping of a Si-CDs aqueous solution at different excitation wavelengths (326–406 nm). (d) The fluorescence decay curve of a Si-CDs aqueous solution (λ_{ex} = 366 nm, λ_{em} = 450 nm).

elements, namely, C, O, N and Si, and the corresponding concentrations are 56.5 %, 17.5 %, 16.7 % and 9.3 %, respectively. Fig. 2**b-d** and Fig. S1 show the high-resolution XPS spectrums (HR-XPS) of C 1s, N 1s, Si 2p, and O 1s, respectively. A divided peak fit to the HR-XPS spectrum of C 1s (Fig. 2**b**) revealed the presence of four peaks at 283.9 eV, 284.7 eV, 285.4 eV, and 287.2 eV, corresponding to the four types of carbon in C–Si, C–C/C═C, C–N/C–O, and C═O, respectively [28,31]. The HR-XPS spectrum of O 1s (Fig. S1) is separated into three peaks at 530.8 eV, 531.6 eV and 532.0 eV, corresponding to the three chemical bonds of C═O, C–O and Si–O [31,32]. The HR-XPS spectrum of N 1s (Fig. 2**c**) could be divided into two peaks at 398.4 eV and 399.3 eV, corresponding to pyridine nitrogen and pyrrole nitrogen, respectively, which indicated that the nitrogen element exists only in two doping sites, pyridine nitrogen and pyrrole nitrogen, was not doped into the graphite lattice to form graphitic nitrogen doping, and is mainly present in the form of pyridine nitrogen [29]. The HR-XPS spectrum of Si 2p (Fig. 2**d**) yielded two peaks at 101.8 eV and 102.3 eV, corresponding to the Si-C and Si–O bonds, respectively [31]. From the above XPS analysis, it is clear that the functional groups presented on the Si-CDs surface might be hydroxyl, silicon hydroxyl, amino, and amide groups, which confirms the analytical results of FT-IR spectra.

Optical properties are an important characteristic of the Si-CDs. Fig. 3**a** shows the absorption spectra of the Si-CDs. The whole absorption spectrum consists of three main components, namely the strongest absorption at 250 nm, a broad absorption peak at 366 nm and a tail-end absorption extending into the visible region. The strongest absorption peak near 250 nm can be attributed to the π-π* transition of the C═C bond, the absorption peak at 366 nm can be ascribed to the n-π* transitions of the C═O and C-N bonds, while the tail-end absorption is assigned to the transition from the n state of the surface functional group to the p* state of the sp^2 domain [33–35]. Fig. 3**b** presents the excitation spectra and emission spectra of the Si-CDs in aqueous solution, from which it can be seen that the Si-CDs could be excited by light in the range of 200–450 nm and their optimal excitation wavelength is 366 nm. Under the excitation wavelength of 366 nm, the emission spectra of the Si-CDs ranged from 400 nm to 600 nm and their fluorescence centers were located around 450 nm. As demonstrated by the photograph of the Si-CDs aqueous solution under UV light irradiation (the inset in Fig. 3**b**), the Si-CDs emitted bright blue light under UV light irradiation. To further investigate the fluorescence properties of the Si-CDs (Fig. S2a), the PL intensity of the maximum emission peak near 450 nm gradually increased when the excitation wavelength was increased from 326 nm to 366 nm; however, the PL intensity of the maximum emission peak near 450 nm gradually decreased when the excitation wavelength was increased from 366 nm to 406 nm. This is because when the Si-CDs are excited at a large wavelength, only a small fraction of the electrons will transit to the excited state and the fluorescence intensity emitted is relatively weak. However, as the excitation wavelength gradually decreases, the excitation energy increases, which favors electrons transition to the excited state, enhancing the fluorescence intensity. Nevertheless, when the excitation wavelength exceeds the optimal excitation wavelength of the Si-CDs, the excitation energy becomes too high, which leads to changes in the internal structure of the Si-CDs. This structural change may lead to a variation in the energy level structure inside the Si-CDs, resulting in a change in the transition path of electrons, or a non-radiative transition of electrons between the ground and excited states, which leads to a decrease in fluorescence efficiency. Furthermore, if the excitation energy is too high, more excitation charges will be generated, which may lead to the destruction of some structures on the surface of the Si-CDs, driven by oxidation or ablation processes, and this will also lead to a gradual weakening of the fluorescence intensity. Therefore, to specifically analyze the excitation-emission correlation of the Si-CDs, a two-dimensional excitation-emission mapping of the Si-CDs was utilized. As shown in Fig. 3**c**, when the excitation varied between 326 and 406 nm, the position of the maximum emission peak of the Si-CDs basically did not vary with the excitation wavelength and remained basically around 450 nm. This experimental evidence indicates that emission is independent from excitation, which may be due to the uniform surface structure and homogeneous particle size of the Si-CDs, which induce a single recombination channel for PL emission [36]. The fluorescence quantum efficiency of the aqueous Si-CD solution is presented in Fig. S2b, and it can be seen that the absolute quantum efficiency of the aqueous Si-CD solution was about 57.8 %. To further investigate the photoluminescence mechanism of the Si-CDs, TCSPC technique was employed to record the fluorescence decay lifetime of the Si-CDs. The PL decay curves of the Si-CDs were fitted using a double exponential function, as described in the Supplementary Information. As illustrated in Fig. 3**d**, the fluorescence lifetime of the prepared Si-CDs was calculated to be 14.3 ns, which is longer compared to the typical lifetime of other CDs in the literature, probably due to the role of the long chain groups on the surface of the Si-CDs to passivate the surface non-radiative defect states and to inhibit the energy transfer between Si-CDs [20,28]. The K_r (radiation rate constant) and K_{nr} (non-radiative rate constant) of Si-CDs were then calculated according to the following equations: [16,27].

$$K_r = \frac{QY}{\tau} \tag{1}$$

$$K_{nr} = \frac{(1 - QY)}{\tau} \tag{2}$$

The values of K_r and K_{nr} for the Si-CDs were calculated as 0.040 and 0.030, respectively. Obviously, K_r was higher than K_{nr} in the Si-CDs, which might be one of the reasons for the high PLQY in the Si-CDs. This evidence suggests that the radiative transition plays a dominant role in the de-excitation paths, leading to the fluorescence generation of Si-CDs. In fact, K_r represents the recombination rate constant through radiative processes (which lead to light emission), while K_{nr} represents the recombination rate through non-radiative processes (which dissipate energy without light emission). These two parameters are related to the PLQY and PL lifetime of CDs. Most of the transition modes of CDs are dominated by radiative transitions, so the higher the K_r, the higher the corresponding PLQYs.

To evaluate the performance of the Si-CDs in LSCs devices, the morphological structure and optical properties of the films prepared by mixing different concentrations of the Si-CDs (0 wt%, 5 wt%, 10 wt%, 25 wt%, 45 wt%, and 70 wt%) with PVA were first investigated. In the process of device fabrication of LSCs, some suitable polymers are usually chosen as film-forming agents, such as polymethyl methacrylate (PMMA), polypropylene (PS), polyvinylpyrrolidone (PVP), polyvinyl alcohol (PVA), etc. These polymers have good solubility in the corresponding solvents, such as PVP dissolves in water, ethanol and methanol, while PVA has good solubility in water and has high light transmission after film formation. Moreover, PVA is rich in hydroxyl groups, which can provide a large number of hydrogen bonds, which can interact with the functional groups on the surface of CDs and form covalent bonds, which is conducive to the immobilization of CDs in the PVA matrix and thus promote the stability of LSCs device performance. According to the SEM images of the Si-CDs/PVA film surfaces (Fig. S3), it can be seen that the pure PVA film surface is very smooth (Fig. S3a); when lower concentrations of Si-CDs are added, the Si-CDs/PVA film surfaces is also smooth without significant changes. However, when the concentration of Si CDs exceeded 25 wt% (Fig. S3d), the Si-CDs/PVA film gradually became rough, which may be due to the strong interaction between Si-CDs and PVA molecules, thereby affecting the surface morphology of the Si-CDs/PVA film. To investigate the dispersion of Si-CDs in the PVA films, EDS analysis was performed on selected areas of the surface of Si-CDs/PVA films (Si-CDs concentration of 25 wt%) using an SEM equipped with an energy spectrometer to obtain the elemental distribution maps. Fig. S4 illustrates the EDS test results of Si-CDs/PVA films with a concentration of 25 wt% of Si-CDs. As shown in Fig. S4e, the main constituent elements in the Si-CDs/PVA films were C, N, O and Si,

whose corresponding elemental concentrations were 52.9 %, 14.2 %, 31.9 % and 1.0 %, respectively. The content of Si element in the Si-CDs/PVA films was small and mainly originated from the organosilylated functional groups on the surface of Si-CDs. Figs. S4a–S4d show the distribution images of C, N, O and Si elements in the Si-CDs/PVA films. The uniform distribution of C, N, O and Si elements in the figures indicates that the Si-CDs exhibits an excellent dispersion in the PVA polymer, which is beneficial to avoid the aggregation-induced fluorescence burst phenomenon of the Si-CDs and thus to prepare high-efficiency LSCs.

To assess the surface morphology and roughness of the Si-CDs/PVA films more visually, the microscopic morphological structure of the Si-CDs/PVA films was investigated by AFM. Fig. 4 exhibits the AFM images of Si-CDs/PVA films with Si-CDs concentrations of 0 wt%, 5 wt%, 10 wt%, 25 wt%, 45 wt% and 70 wt%, respectively. It is clearly seen that the surface of Si-CDs/PVA films is highly affected by the presence of Si-CDs, which induce strong surface modification as the concentration of Si-CDs increased. In particular, up to 10 wt%, no significant difference is recorded. At higher concentrations, pores are forming, whose dimensions increase with the increasing Si-CDs concentration. In the sample with the highest Si-CDs concentration large micrometer-sized pores appear. The AFM 3D morphology of the Si-CDs/PVA film in Fig. S5 clearly revealed the difference of the Si-CDs/PVA film surface with clear porosity. Furthermore, the effect of the Si-CDs concentration on the surface morphology of Si-CDs/PVA films was investigated by AFM calculation of surface roughness (R_q). The roughness of Si-CDs/PVA films varies (Fig. S4): the R_q value of pure PVA films is 0.34 nm, which indicates that the surface is very smooth. With the increasing concentration of Si-CDs doping, the R_q value of Si-CDs/PVA films also increased, reaching the value of 119 nm. This result is almost consistent with the SEM surface morphology structure, which also fully reflected the interaction between Si-CDs and PVA, which seriously affects the surface morphology of the Si-CDs/PVA films at high Si-CDs concentration. To adequately demonstrate the interaction between Si-CDs and PVA, the Si-CDs/PVA films were characterized employing XRD and FTIR. Fig. S6a shows the XRD patterns of the Si-CDs/PVA films with pure PVA and different Si-CDs concentrations. In the XRD image of the pure PVA, a diffraction peak at $2\theta \approx 19.7^\circ$ corresponding to its (101) plane exists, and two diffraction peaks at about 22.8° and 40.6° for PVA, corresponding to its (200) and (111) planes, respectively [37]. The diffraction peaks at 19.7° and 22.8° were combined into a single diffraction peak when the crystallinity of PVA was low. As the concentration of Si-CDs increases, the sharp, high-intensity diffraction peak at 19.7° of the Si-CDs/PVA film gradually became a broad, low-intensity diffraction peak, and the two diffraction peaks at 22.8° and 40.6° gradually disappear, indicating that the crystallinity of the Si-CDs/PVA film decreases with the increase of Si-CDs concentration, which is consistent with the results of AFM analysis. The PVA is a semi-crystalline polymer, therefore, the interaction between Si-CDs and PVA will affect the crystallinity of Si-CDs/PVA films. The crystallinity of Si-CDs/PVA films was lower than that of pure PVA due to the interaction between Si-CDs and PVA molecules, which prevented PVA molecules from forming crystalline regions in an orderly arrangement [37,38]. From the above analytical results, it is clear the presence of an interaction force between the Si-CDs and PVA molecules. Moreover, there were a large number of hydroxyl groups in PVA, which also formed hydrogen bonding interactions with the Si-CDs. It can be inferred that the bonding structure between Si-CDs and PVA is shown in Fig. S6b, where the Si-CDs and PVA are cross-linked by chemical bonding and hydrogen bonding to form Si-CDs/PVA films by reaction. The aggregation-induced fluorescence quenching phenomenon of Si-CDs could be greatly suppressed in this way, thus increasing the loading of Si-CDs in the films for the preparation of high-efficiency LSCs.

Furthermore, the interaction between the Si-CDs and PVA was discovered to have a good UV shielding absorption function. As shown in Fig. 5**a**, when a blank glass sheet or pure PVA is used to separate the pure Si-CDs solution and the 365 nm UV light source, the Si-CDs solution emits bright blue fluorescence, while when the Si-CDs combined with PVA is used as a separator in the same way, the mixed solution of Si-CDs and PVA absorbs UV light very well. This revealed that the combination of Si-CDs and PVA has excellent shielding absorption properties for UV light. To further investigate the UV shielding absorption performance of the Si-CDs/PVA composite, thin film LSCs were prepared by mixing different concentrations of Si-CDs (5 wt%, 10 wt%, 25 wt%, 45 wt% and 70 wt%) with PVA using drop coating method, as shown in Fig. 5**c**. As shown in Fig. 5**d**, except for the blank control sample (0 wt%), the

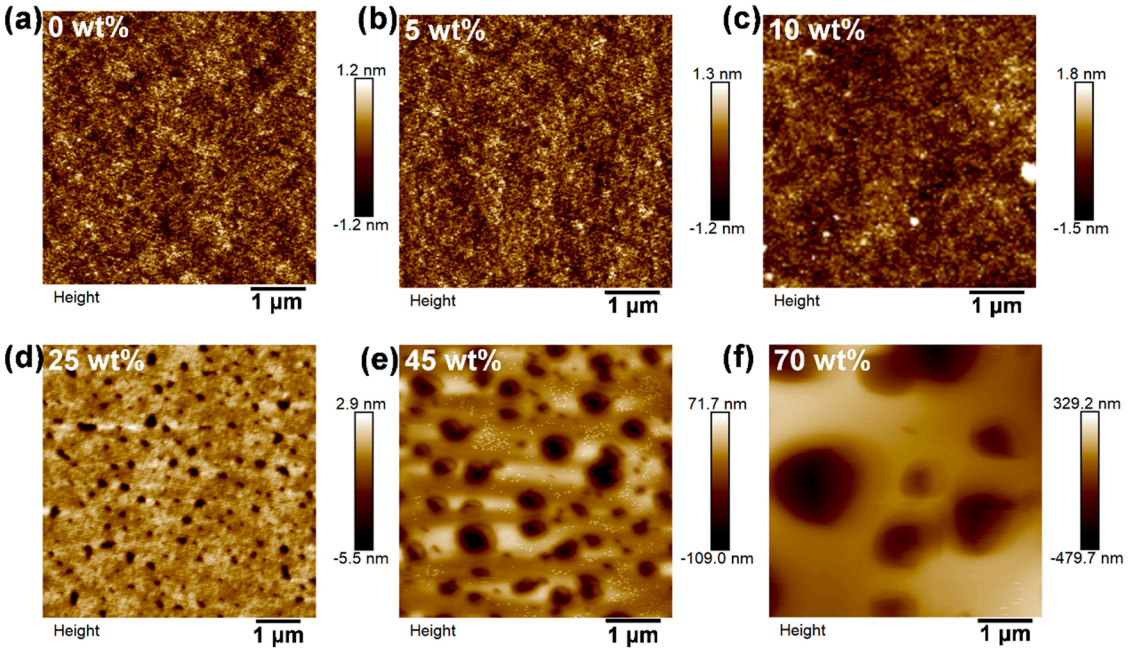

Fig. 4. AFM topographical images of Si-CDs/PVA films with the concentrations of Si-CDs of (a) 0 wt%, (b) 5 wt%, (c) 10 wt%, (d) 25 wt%, (e) 45 wt%, and (f) 70 wt %, respectively.

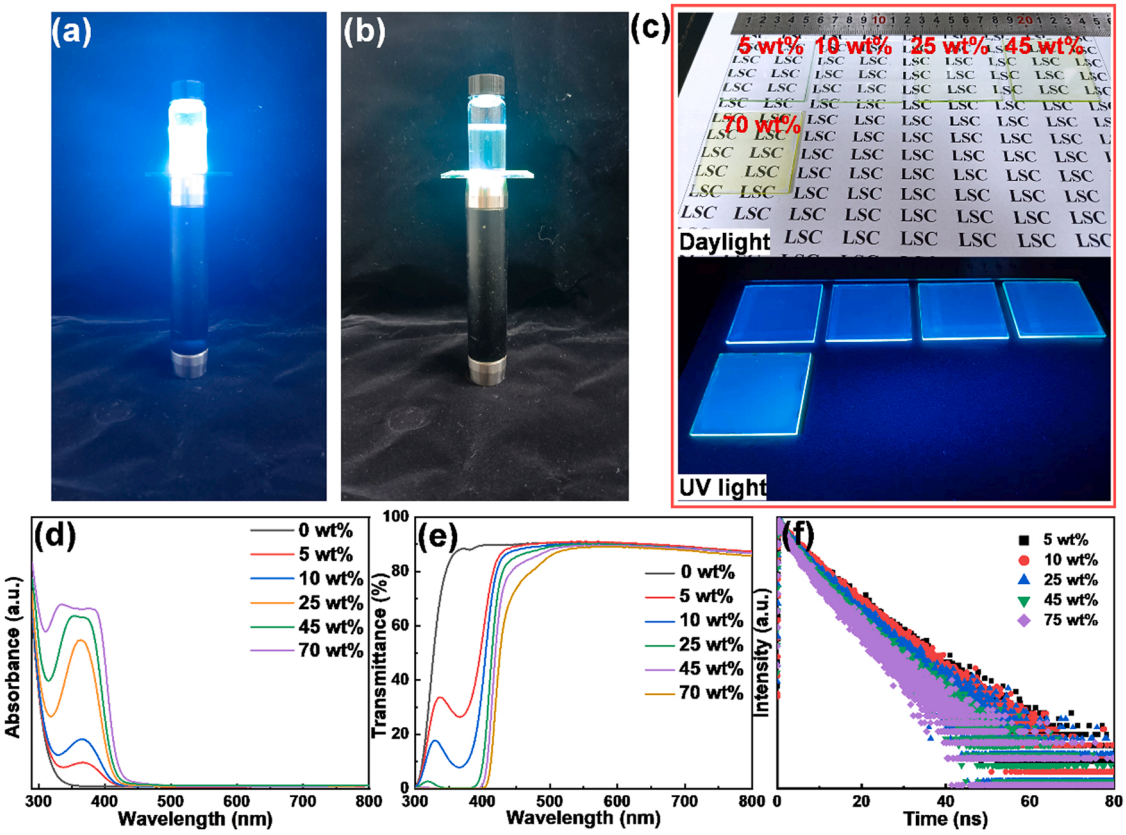

Fig. 5. (a) Si-CDs solution and UV light source were separated by a blank glass sheet. (b) Si-CDs solution and UV light source were separated by the Si-CDs/PVA based LSC (the concentration of Si-CDs was 25 wt%). (c) Photographs of the Si-CDs/PVA based LSC with the concentrations of Si-CDs of 5 wt%, 10 wt%, 25 wt %, 45 wt% and 70 wt% under daylight and UV light, respectively. (d) UV–vis absorption spectra and (e) Transmittance spectra of the Si-CDs/PVA based LSC with the concentrations of Si-CDs of 0 wt%, 5 wt%, 10 wt%, 25 wt%, 45 wt% and 70 wt%, respectively. (f) The time-resolved PL decay curves of the Si-CDs/PVA based LSC with various concentrations of Si-CDs.

absorption range of all Si-CDs/PVA thin film LSCs was between 300 nm and 450 nm, and the characteristic absorption peaks were all located near 365 nm, exhibiting strong absorption in the UV band. With the increase of Si-CDs concentration, the light absorption of Si-CDs/PVA film-type LSCs in the range of 300–450 nm increased, which indicates that the high Si-CDs concentration in the films is beneficial to enhance the light absorption of Si-CDs/PVA film-based LSCs. Fig. 5**e** shows the transmission spectra of the corresponding Si-CDs/PVA films. Compared with the blank control sample (0 wt%), the other Si-CDs/PVA film-type LSCs exhibited a decrease in light transmission at around 365 nm, and their transmission of UV light continuously decreased with the increase of the concentration of Si-CDs. This is because the characteristic absorption peak of Si-CDs is located near 365 nm, and with the increase of Si-CDs concentration, the absorption ability of the CDs/PVA film-type LSC for light around 365 nm increases, resulting in a decrease of its transmittance, which is consistent with the UV–visible absorption spectrum of the Si-CDs/PVA film-type LSC. Fig. S7 shows the relationship between the Si-CDs concentration and the transmission rates of ultraviolet (UV) (350 nm) and visible (540 nm) light, from which it can be seen that when the Si-CDs doping concentration is 25 wt%, the transmission rate of Si-CDs/PVA film-type LSC for UV is close to 0, i.e., almost full absorption occurs. However, with the increase of Si-CDs doping concentration, the light transmittance of Si-CDs/PVA thin-film LSC in the visible range remained almost unchanged at about 90 %. The above results show that Si-CDs/PVA thin-film LSCs are compatible with buildings that need light, such as windows, to absorb UV radiation and use it for solar power generation as well as to meet the need for high light transmission in the visible range. Based on the correlated PL performance of Si-CDs/PVA film-based LSCs (Fig. S8), the fluorescence intensity of Si-CDs/PVA film-based LSCs with different Si-CDs concentrations increased and then decreased by increasing the excitation wavelength, revealing that the optimal excitation wavelength exists in the range of 320–410 nm, and all the samples exhibit excitation-emission independent property. As illustrated in Fig. S8f, the optimal excitation wavelength and the most intense emission peak of Si-CDs/PVA thin-film LSCs were red-shifted by approximately 19 nm and 11 nm, respectively, as the concentration of Si-CDs increases from 5 wt % to 70 wt%. There are two main possible reasons for the red-shift of excitation and emission spectra with the increase of Si-CDs doping concentration: namely, the reabsorption effect and the concentration-induced fluorescence quenching-related Förster resonance energy transfer (FRET) process [20,21]. It can be seen that the fluorescence intensity increased and then decreased as the concentration of the Si-CDs increased and reaches a maximum when the loading of Si-CDs in the film is up to 25 %. Combined with the previous related characterization, our synthetic strategy allows to increase the loading of Si-CDs by chemically dispersing them in the PVA matrix, and the optimal loading is around 25 %. However, the fluorescence intensity decreased above the optimal concentration. Notably, the reabsorption effect does not affect the exciton dynamics of the fluorescent material and only redshifts the spectra without altering their fluorescence lifetimes, while the FRET process not only redshifts the spectra but also shortens the fluorescence lifetimes due to the introduction of additional non-radiative pathways [39,40]. Since the non-negligible overlap of the absorption and emission spectra of Si-CDs leads to a reabsorption effect, to further evaluate the presence of the FRET process, the time-resolved PL decay curves of Si-CDs/PVA film-based LSCs with different Si-CDs concentrations was investigated. As shown in Fig. 5**f**, the time-resolved PL decay curves of

the Si-CDs/PVA film-type LSCs with different Si-CDs concentrations differ. Table S1 displays a slight decrease in the fluorescence lifetime time of the Si-CDs/PVA film-type LSCs with increasing the concentration of Si-CDs, which indicated a slight increase in the additional non-radiative pathway introduced by the FRET process. Therefore, in addition to the reabsorption effect, a FRET process is also present, inducing the red-shift of the absorption and emission spectra and the decrease of the fluorescence intensity.

Similarly, the thickness of the Si-CDs/PVA thin-film LSCs is a key parameter influencing the overall device performance. The thickness of Si-CDs/PVA thin-film LSCs was investigated by fixing the loading of the Si-CDs (Si-CDs concentration of 25 wt% was selected, which exhibits the best optical performances) and adjusting the drop volume used in the drop coating process (1 mL, 1.5 mL, 2 mL, 2.5 mL and 3 mL, respectively). It can be seen from the SEM images (Fig. S9) that the film thickness of the Si-CDs/PVA film-type LSC increased with the increase of the drop coating volume of the Si-CDs/PVA mixture, and the film thicknesses of the Si-CDs/PVA film-type LSC with the drop coating volumes of 1 mL, 1.5 mL, 2 mL, 2.5 mL and 3 mL of the Si-CDs/PVA mixture were 28 μm, 37 μm, 52.65 μm, 80.17 μm, and 112.85 μm, respectively. Fig. S10a shows the optical pictures of the LSCs prepared using different drop volumes. The Si-CDs/PVA thin-film LSCs with different film thicknesses showed very high transparency and the degree of staining (yellow-green color) of the Si-CDs/PVA thin-film LSCs increased with the increase of the film thickness. Under UV light irradiation, the Si-CDs/PVA thin-film LSCs also emit bright blue light around the film. Additionally, the optical properties of the LSC devices were characterized using PL, as can be observed in Fig. S10b, where the fluorescence emission intensity first increases and then decreases with the increase of the film thickness, reaching the optimum at the drop coating volume of 2 mL. This indicates that increasing the film thickness can improve the fluorescence intensity of the Si-CDs/PVA film-based LSCs to a certain extent, but thicker films perform worse. It is worth noting that the change in film thickness did not cause a shift in the fluorescence emission peak position, but has an effect on the fluorescence intensity (Fig. S11a). The LSCs with different film thicknesses also exhibited absorption of light in the range of 300–450 nm, and the characteristic absorption peak remained close to 365 nm (Fig. S10c). This is mainly attributed to the fact that an increase in film thickness will lead to an increase in the number of Si-CDs in the film, which will increase the absorbance of LSCs. Strikingly, as shown in Fig. S10d, the transmittance spectra of Si-CDs/PVA film-based LSCs in the range 400–800 nm did not show a very significant change with increasing film thickness. Fig. S11b shows that the UV transmittance of the Si-CDs/PVA film type LSC was almost 0 for all film thicknesses, while the visible light transmittance also remained almost unchanged at about 90 %. This is

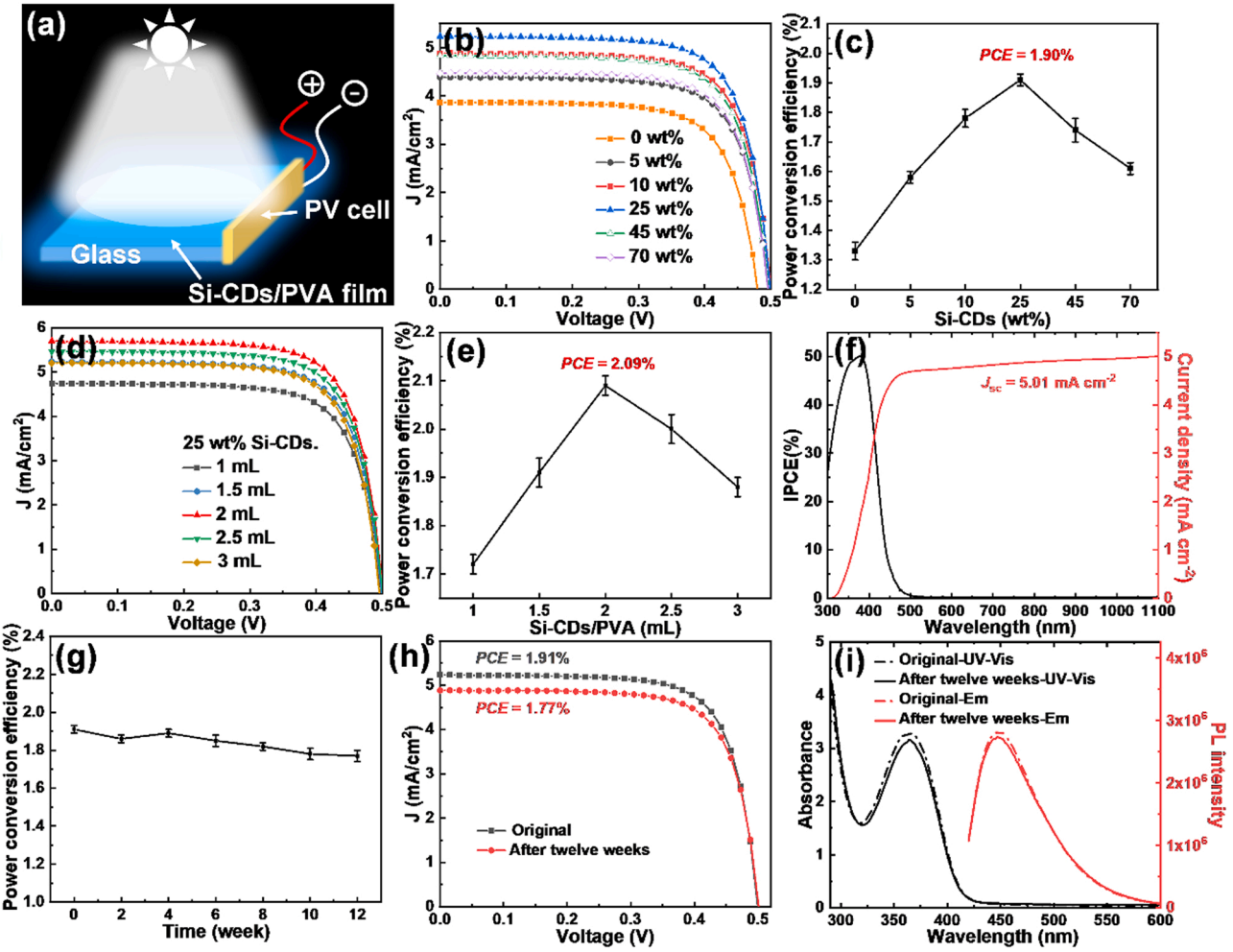

Fig. 6. (a) Schematic diagram of LSCs. (b) *J-V* curves and (c) PCE of Si-CDs/PVA based LSC with various concentrations of Si-CDs. (d) *J-V* curves and (e) PCE of Si-CDs/PVA based LSC (the concentration of Si-CDs was 25 wt%) with various drop volumes of Si-CDs/PVA mixture. (f) EQE and corresponding integrated current density of Si-CDs/PVA based LSC (the concentration of Si-CDs was 25 wt%). (g) PCE and (h) *J-V* curves of Si-CDs/PVA based LSC (the concentration of Si-CDs was 25 wt%) before and after 12 weeks of storage under natural conditions. (i) UV–vis absorption and emission spectra of Si-CDs/PVA based LSC (the concentration of Si-CDs was 25 wt%) before and after 12 weeks of storage under natural conditions.

mainly due to the high loading concentration of Si-CDs (25 wt%), which absorbs UV almost completely (almost zero transmittance), so that the increase in film thickness does not change the transmittance in this band. In addition, Si-CDs hardly absorbs light in the visible range and the PVA film itself has high transparency, which makes the change of Si-CDs concentration and film thickness not affecting the transmittance of Si-CDs/PVA film type LSC in the visible range.

To evaluate the performance of the LSCs devices, PCE measurements were performed. A simple scheme is shown in Fig. 6**a** for the *J-V* curves and PCE of the Si-CDs/PVA thin-film type LSC measured under a standard solar light (AM 1.5 G, 100 mW cm^{-2}). Fig. 6**b** shows the *J-V* curves corresponding to different concentrations of Si-CDs. The photocurrent density of Si-CDs/PVA thin-film LSCs exhibits a clear trend with concentration: it first increases and then it decreases as the concentration of Si-CDs increases. The PCE and η_{opt} also show the same trend (Fig. 6**c**). When the doping concentration of Si-CDs increases to 25 %, the PCE of Si-CDs/PVA thin-film LSCs reaches a maximum value (1.90 %), while the values of J_{sc}, V_{oc} and η_{opt} are 5.24 mA cm^{-2}, 0.50 V and 1.98 %, respectively. The specific relevant parameters are shown in Table S2. The main reason for this incremental change is that the increase in the number of Si-CDs in the film increases the absorbance of the Si-CDs/PVA film type LSCs, and the consequent emission. This way, the number of waveguided photons increase accordingly, improving the PCE of the Si-CDs/PVA film. However, above a concentration threshold, the PCE decreases, which is mainly due to the reabsorption effect and the FRET process leading to the reduction of fluorescence intensity. Similarly, device performance is also presented in Fig. 6**d**, 6**e** for different drop loading amounts. The PCE reaches its maximum value at the drop loading volume of 2 mL, which corresponds to PCE, J_{sc}, V_{oc} and η_{opt} values of 2.09 %, 5.70 mA cm^{-2}, 0.50 V and 2.16 %, respectively. The relevant parameters are shown in Table S3. Furthermore, the optical responsiveness of the Si-CDs/PVA thin-film LSCs to different wavelengths was investigated by characterizing the external quantum efficiency (EQE) of Si-CDs/PVA thin-film LSC (with a concentration of 25 wt% of Si-CDs). As illustrated in Fig. 6**f**, the EQE spectra of the Si-CDs/PVA thin-film LSCs are similar to their UV-Vis absorption spectra, responding in the wavelength range of 300–500 nm, and the peak of the EQE maximum is at 366 nm. The current density obtained by integrating the EQE spectra is 5.01 mA cm^{-2}, which is consistent with the measured J_{sc}.

Besides the photovoltaic performance, the environmental stability is also one of the key properties of the LSCs. The changes of UV–vis absorption spectra, emission spectra and photovoltaic properties of Si-CDs/PVA thin film LSCs with a concentration of 25 wt% of the Si-CDs and a drop volume of 1 mL of Si-CDs/PVA mixture were investigated before and after storage under natural conditions for 12 weeks to investigate the environmental stability of LSCs. As shown in Fig. 6**g**, 6**h**, the J_{sc} of Si CDs/PVA thin film LSC slightly decreased, and its PCE decreased from 1.91 % to 1.77 %: only a decrease of 7.3 % after 12 weeks of storage under natural conditions. As shown in Fig. 6**i**, the UV visible absorption and emission spectra of Si CDs/PVA thin film LSC showed almost no changes in peak shape and position compared to the initial one, except for a decrease in absorbance and PL intensity. The above analysis indicated that Si-CDs/PVA thin film LSC has excellent stability.

4. Conclusion

A kind of organosilane-grafted CDs with UV shielding property were designed and dispersed in a PVA matrix to prepare highly transparent and highly loaded LSC devices. The synthesized Si-CDs have a quasi-spherical structure with an average particle size of about 4.35 nm. The fluorescence emission wavelength reaches its maximum at 450 nm when the excitation wavelength is 366 nm, and the PLQY is as high as 57.8 %. We investigated the interaction between Si-CDs and PVA, and we found that Si-CDs possess excellent UV shielding properties after interacting with PVA. The effects of different loading concentrations of Si-CDs and the thickness of the films on the LSCs devices were analyzed in detail, and the experimental conditions were finally optimized to obtain LSC devices with Si-CDs loading up to 25 wt% with transparency above 90 % in the visible range (400 – 800 nm), while the maximum PCE was 2.09 %. Finally, the environmental stability of the LSCs devices was investigated, and the good optical and device properties were maintained even after 12 weeks. This synthetic strategy is expected to provide favorable technical support for future LSC device fabrication and pave the way for the development of CDs-based LSC devices.

CRediT authorship contribution statement

Jiurong Li: Methodology, Formal analysis, Validation, Data curation, Writing – original draft, Review & editing. **Jiancang Chen:** Formal analysis, Validation, Data curation. **Xiujian Zhao:** Review & editing. **Alberto Vomiero:** Conceptualization, Review & editing, Funding acquisition, Project administration. **Xiao Gong:** Conceptualization, Supervision, Review & editing, Funding acquisition, Project administration.

Declaration of Competing Interest

The authors declare that they have no known competing financial interests or personal relationships that could have appeared to influence the work reported in this paper.

Data availability

Data will be made available on request.

Acknowledgements

This work was supported by the National Natural Science Foundation of China (No. 21774098), and the Ministry of Education, China - 111 Project (No. B18038). A. Vomiero acknowledges the Kempe Foundation, the Wallenberg Foundation and LTU Lab fund for financial support.

Appendix A. Supporting information

Supplementary data associated with this article can be found in the online version at doi:10.1016/j.nanoen.2023.108674.

References

[1] Y. Zhou, H. Zhao, D. Ma, F. Rosei, Harnessing the properties of colloidal quantum dots in luminescent solar concentrators, Chem. Soc. Rev. 47 (15) (2018) 5866–5890.
[2] R. Mazzaro, A. Vomiero, The renaissance of luminescent solar concentrators: the role of inorganic nanomaterials, Adv. Energy Mater. 8 (33) (2018) 1801903.
[3] J. Roncali, Luminescent solar collectors: Quo Vadis? Adv. Energy Mater. 10 (36) (2020) 2001907.
[4] H. Zhao, G. Liu, S. You, F.V.A. Camargo, M. Zavelani-Rossi, X. Wang, C. Sun, B. Liu, Y. Zhang, G. Han, A. Vomiero, X. Gong, Gram-scale synthesis of carbon quantum dots with a large Stokes shift for the fabrication of eco-friendly and high-efficiency luminescent solar concentrators, Energy Environ. Sci. 14 (1) (2021) 396–406.
[5] J. Li, H. Zhao, X. Zhao, X. Gong, Red and yellow emissive carbon dots integrated tandem luminescent solar concentrators with significantly improved efficiency, Nanoscale 13 (21) (2021) 9561–9569.
[6] S. Castelletto, A. Boretti, Luminescence solar concentrators: a technology update, Nano Energy 109 (2023), 108269.
[7] G. Liu, H. Zhao, F. Diao, Z. Ling, Y. Wang, Stable tandem luminescent solar concentrators based on CdSe/CdS quantum dots and carbon dots, J. Mater. Chem. C 6 (37) (2018) 10059–10066.
[8] X. Liu, D. Benetti, J. Liu, L. Jin, F. Rosei, Color-tunable multilayered laminated luminescent solar concentrators based on colloidal quantum dots, Nano Energy 111 (2023), 108438.
[9] Y. Li, P. Miao, W. Zhou, X. Gong, X. Zhao, N-doped carbon-dots for luminescent solar concentrators, J. Mater. Chem. A 5 (40) (2017) 21452–21459.
[10] Y. Zhou, D. Benetti, X. Tong, L. Jin, Z.M. Wang, D. Ma, H. Zhao, F. Rosei, Colloidal carbon dots based highly stable luminescent solar concentrators, Nano Energy 44 (2018) 378–387.

[11] G. Liu, X. Wang, G. Han, J. Yu, H. Zhao, Earth abundant colloidal carbon quantum dots for luminescent solar concentrators, Mater. Adv. 1 (2) (2020) 119–138.
[12] J. Wang, J. Wang, Y. Xu, J. Jin, W. Xiao, D. Tan, J. Li, T. Mei, L. Xue, X. Wang, Controlled synthesis of long-wavelength multicolor-emitting carbon dots for highly efficient tandem luminescent solar concentrators, ACS Appl. Energy Mater. 3 (12) (2020) 12230–12237.
[13] L. ZdraZil, S. Kalytchuk, K. Hola, M. Petr, O. Zmeskal, S. Kment, A.L. Rogach, R. Zboril, A carbon dot-based tandem luminescent solar concentrator, Nanoscale 12 (12) (2020) 6664–6672.
[14] Y. Han, X. Zhao, A. Vomiero, X. Gong, H. Zhao, Red and green-emitting biocompatible carbon quantum dots for efficient tandem luminescent solar concentrators, J. Mater. Chem. C 9 (36) (2021) 12255–12262.
[15] J. Chen, H. Zhao, Z. Li, X. Zhao, X. Gong, Highly efficient tandem luminescent solar concentrators based on eco-friendly copper iodide based hybrid nanoparticles and carbon dots, Energy Environ. Sci. 15 (2) (2022) 799–805.
[16] J. Li, H. Zhao, X. Zhao, X. Gong, Boosting efficiency of luminescent solar concentrators using ultra-bright carbon dots with large Stokes shift, Nanoscale Horiz. 8 (1) (2022) 83–94.
[17] G. Liu, M. Zavelani-Rossi, G. Han, H. Zhao, A. Vomiero, Red-emissive carbon quantum dots enable high efficiency luminescent solar concentrators, J. Mater. Chem. A 11 (16) (2023) 8950–8960.
[18] Y. Han, L. Liccardo, E. Moretti, H. Zhao, A. Vomiero, Synthesis, optical properties and applications of red/near-infrared carbon dots, J. Mater. Chem. C 10 (33) (2022) 11827–11847.
[19] Y. Wu, L. Zhao, X. Cao, Y. Zhang, X. Jiang, Z. Sun, Y. Zhan, Bright and multicolor emissive carbon dots/organosilicon composite for highly efficient tandem luminescent solar concentrators, Carbon 207 (2023) 77–85.
[20] M.J. Talite, H.Y. Huang, K.B. Cai, K.C. Capinig, Co, P.A. Cynthia Santoso, S. H. Chang, W.C. Chou, C.T. Yuan, Visible-transparent luminescent solar concentrators based on carbon nanodots in the siloxane matrix with ultrahigh quantum yields and optical transparency at high-loading contents, J. Phys. Chem. Lett. 11 (2) (2020) 567–573.
[21] M.J. Talite, H.Y. Huang, Y.H. Wu, P.G. Sena, K.B. Cai, T.N. Lin, J.L. Shen, W. C. Chou, C.T. Yuan, Greener luminescent solar concentrators with high loading contents based on in situ cross-linked carbon nanodots for enhancing solar energy harvesting and resisting concentration-induced quenching, ACS Appl. Mater. Interfaces 10 (40) (2018) 34184–34192.
[22] J. Wu, W. Xin, Y.H. Wu, Y. Zhan, J.H. Li, J.Y. Wang, S.Q. Huang, X.B. Wang, Solid-state photoluminescent silicone-carbon dots/dendrimer composites for highly efficient luminescent solar concentrators, Chem. Eng. J. 422 (2021), 130158.
[23] S. Lu, L. Sui, J. Liu, S. Zhu, A. Chen, M. Jin, B. Yang, Near-infrared photoluminescent polymer-carbon nanodots with two-photon fluorescence, Adv. Mater. 29 (15) (2017) 1603443.
[24] J. Liu, Y. Geng, D. Li, H. Yao, Z. Huo, Y. Li, K. Zhang, S. Zhu, H. Wei, W. Xu, J. Jiang, B. Yang, Deep red emissive carbonized polymer dots with unprecedented narrow full width at half maximum, Adv. Mater. 32 (17) (2020) 1906641.
[25] Q. Zhang, R. Wang, B. Feng, X. Zhong, K.K. Ostrikov, Photoluminescence mechanism of carbon dots: triggering high-color-purity red fluorescence emission through edge amino protonation, Nat. Commun. 12 (1) (2021) 6856.
[26] J. Guo, Y. Lu, A.Q. Xie, G. Li, Z.B. Liang, C.F. Wang, X. Yang, S. Chen, Yellow-emissive carbon dots with high solid-state photoluminescence, Adv. Funct. Mater. 32 (20) (2022) 2110393.
[27] Z. Wan, Y. Li, Y. Zhou, D. Peng, X. Zhang, J. Zhuang, B. Lei, Y. Liu, C. Hu, High-efficiency solid-state luminescence from hydrophilic carbon dots with aggregation-induced emission characteristics, Adv. Funct. Mater. (2023) 2207296.
[28] J. Zheng, Y. Wang, F. Zhang, Y. Yang, X. Liu, K. Guo, H. Wang, B. Xu, Microwave-assisted hydrothermal synthesis of solid-state carbon dots with intensive emission for white light-emitting devices, J. Mater. Chem. C. 5 (32) (2017) 8105–8111.
[29] J. Liu, D. Li, K. Zhang, M. Yang, H. Sun, B. Yang, One-step hydrothermal synthesis of nitrogen-doped conjugated carbonized polymer dots with 31% efficient red emission for in vivo imaging, Small 14 (15) (2018) 1703919.
[30] F. Yuan, Z. Wang, X. Li, Y. Li, Z. Tan, L. Fan, S. Yang, Bright multicolor bandgap fluorescent carbon quantum dots for electroluminescent light-emitting diodes, Adv. Mater. 29 (3) (2017) 1604436.
[31] B.K. Barman, Ø.S. Handegård, D. Hernández-Pinilla, S.L. Shinde, T. Nagao, Transparent hard coatings with SiON-encapsulated N-doped carbon dots for complete UV blocking and white light emission, ACS Appl. Electron. Mater. 3 (9) (2021) 3761–3773.
[32] B.E. Kwak, H.J. Yoo, D.H. Kim, Encapsulation of carbon dots in silica matrices offers narrow emission in the solid-state of printed fluorescent inks, ACS Appl. Nano Mater. 4 (9) (2021) 9497–9507.
[33] C.-L. Shen, J.-H. Zang, Q. Lou, L.-X. Su, Z. Li, Z.-Y. Liu, L. Dong, C.-X. Shan, In-situ embedding of carbon dots in a trisodium citrate crystal matrix for tunable solid-state fluorescence, Carbon 136 (2018) 359–368.
[34] A. Sharma, T. Gadly, S. Neogy, S.K. Ghosh, M. Kumbhakar, Molecular origin and self-assembly of fluorescent carbon nanodots in polar solvents, J. Phys. Chem. Lett. 8 (5) (2017) 1044–1052.
[35] S. Saxena, T.A. Tyson, S. Shukla, E. Negusse, H. Chen, J. Bai, Investigation of structural and electronic properties of graphene oxide, Appl. Phys. Lett. 99 (1) (2011), 013104.
[36] Y. Liu, J. Wei, X. Yan, M. Zhao, C. Guo, Q. Xu, Barium charge transferred doped carbon dots with ultra-high quantum yield photoluminescence of 99.6% and applications, Chin. Chem. Lett. 32 (2) (2021) 861–865.
[37] H. Pingan, J. Mengjun, Z. Yanyan, H. Ling, A silica/PVA adhesive hybrid material with high transparency, thermostability and mechanical strength, RSC Adv. 7 (5) (2017) 2450–2459.
[38] L. Chen, K. Zheng, X. Tian, K. Hu, R. Wang, C. Liu, Y. Li, P. Cui, Double glass transitions and interfacial immobilized layer in in-situ-synthesized poly(vinyl alcohol)/silica nanocomposites, Macromolecules 43 (2) (2009) 1076–1082.
[39] S.A. Crooker, J.A. Hollingsworth, S. Tretiak, V.I. Klimov, Spectrally resolved dynamics of energy transfer in quantum-dot assemblies: towards engineered energy flows in artificial materials, Phys. Rev. Lett. 89 (18) (2002), 186802.
[40] D. Qu, D. Yang, Y. Sun, X. Wang, Z. Sun, White emissive carbon dots actuated by the H-/J-aggregates and forster resonance energy transfer, J. Phys. Chem. Lett. 10 (14) (2019) 3849–3857.

Jiurong Li is currently pursuing his Ph.D. degree at the State Key Laboratory of Silicate Materials for Architectures, Wuhan University of Technology. After he received his B.S. degree from Ningbo University in 2019, he joined Professor Xiao Gong's group to start his research journey. Currently, his research interest is focused on multifunctional materials, especially the development of synthesis methods for fluorescent nano-materials and their applications.

Jiancang Chen received his master's degree from the State Key Laboratory of Silicate Materials for Architectures, Wuhan University of Technology. His research interest is focused on synthesis and application of the fluorescent nano-materials.

Xiujian Zhao is a Chief Professor at Wuhan University of Technology, China. He was the head of the State Key Laboratory of Silicate Materials for Architectures. His current research is focused on glass, functional films; and functional nanomaterials.

Alberto Vomiero is a chair professor in Experimental Physics at the Department of Engineering Sciences and Mathematics, Luleå University of Technology, Sweden and a professor in Industrial Engineering at the Department of Molecular Sciences and Nanosystems, Ca' Foscari University of Venice, Italy. He is leading a multidisciplinary group focusing on the development of advanced nanomaterials for energy and environmental applications, including solar cells, water splitting and photocatalysis. He is a former Marie Curie International Outgoing Fellow of the European Commission, Fellow of the Swedish Foundations, of the American Ceramic Society, of the Royal Society of Chemistry, and several other Societies.

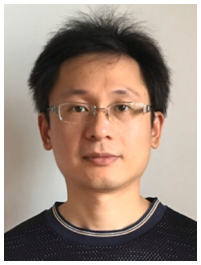

Xiao Gong is a Professor in the State Key Laboratory of Silicate Materials for Architectures, Wuhan University of Technology, China. He received his Ph.D. in materials science from Zhejiang University. Prior to joining Wuhan University of Technology, he was a postdoctoral associate at the University of Pittsburgh, USA. He is in the Editorial Advisory Board of *Langmuir*. His current research is focused on polymer composite films; colloid surface and interface chemistry; functional nanomaterials; synthesis and application of the fluorescent materials.